JACS
JOURNAL OF THE AMERICAN CHEMICAL SOCIETY

Article

pubs.acs.org/JACS

Size-Controlled Nanoparticle-Guided Assembly of Block Copolymers for Convex Lens-Shaped Particles

Kang Hee Ku,[†] Jae Man Shin,[†] Minsoo P. Kim,[†] Chun-Ho Lee,[‡] Min-Kyo Seo,[‡] Gi-Ra Yi,[§] Se Gyu Jang,*[,∥] and Bumjoon J. Kim*[,†]

[†]Department of Chemical and Biomolecular Engineering, [‡]Department of Physics, Korea Advanced Institute of Science and Technology (KAIST), Daejeon, 305-701 Republic of Korea

[§]School of Chemical Engineering, Sungkyunkwan University, Suwon, 440-746 Republic of Korea

[∥]Korea Electric Power Research Institute (KEPRI), Daejeon, 305-760 Republic of Korea

Supporting Information

ABSTRACT: The tuning of interfacial properties at selective and desired locations on the particles is of great importance to create the novel structured particles by breaking the symmetry of their surface property. Herein, a dramatic transition of both the external shape and internal morphology of the particles of polystyrene-*b*-poly(4-vinylpyridine) (PS-*b*-P4VP) was induced by precise positioning of size-controlled Au nanoparticle surfactants (Au NPs). The size-dependent assembly of the Au NPs was localized preferentially at the interface between the P4VP domain at the particle surface and the surrounding water, which generated a balanced interfacial interaction between two different PS/P4VP domains of the BCP particles and water, producing unique convex lens-shaped BCP particles. In addition, the neutralized interfacial interaction, in combination with the directionality of the solvent-induced ordering of the BCP domains from the interface of the particle/water, generated defect-free, vertically ordered porous channels within the particles. The mechanism for the formation of these novel nanostructures was investigated systemically by varying the size and the volume fraction of the Au NPs. Furthermore, these convex lens-shaped particles with highly ordered channels can be used as a microlens, in which the light can be concentrated toward the focal point with enhanced near-field signals. And, these particles can possess additional optical properties such as unique distribution of light scattering as a result of the well-ordered Au cylinders that filled into the channels, which hold great promise for use in optical, biological-sensing, and imaging applications.

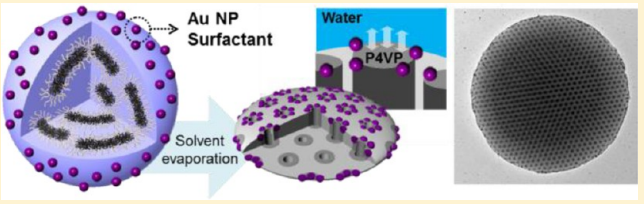

INTRODUCTION

Three-dimensional confinement is a powerful tool for breaking the symmetry of a structure, thus creating novel structured materials that are not available in bulk.[1−4] Self-assembly of block copolymers (BCPs) confined in a small droplet can generate nanostructured particles with tunable internal structures, shapes, and surface properties, thus giving rise to potential applications in a particle-based technologies such as photonic bandgap materials,[5] optochemical sensing devices,[6] and catalytic supports.[7,8] The control of the interfacial interactions between the BCP particles and the surrounding media is critical in determining the morphology within this confined geometry. In addition, the mobile interfacial boundary of the emulsion particle, which is controlled by the nature of the surfactants, can further expand the richness of their morphological behavior.[2,9−12] For example, Yang et al. developed an elegant route of using mixed surfactants to control the dynamics of the mobile interface between the BCP particles and the surrounding medium, producing unique structured BCP particles.[9] Recently, Jang et al. demonstrated that the interfacial interactions at the surface of BCP particle can be modulated by addition of polymer-coated nanoparticles (NPs), producing very interesting structures of ellipsoidal particles of symmetric BCPs.[11] The development of such anisotropic structures of the particles requires precise tuning in the dynamics of the interfacial boundary, but it is extremely challenging to control the interfacial properties at different locations of the particle independently. The precise positioning of two different surfactants at selective and desirable locations on the particle surface can be a key technique to address these issues.

For the coassembly of functional inorganic NPs and BCPs, nanostructured BCP domains act as a scaffold that directs not only the position of NPs but also their orientation and three-dimensional arrangement,[13−24] which can be achieved by controlling the interplay of enthalpic interactions between the NPs and BCPs and entropy loss of the chains wrapping the NPs.[25−27] Conversely, if the location of the NPs can be precisely controlled within the polymeric domain, they can affect the morphological behavior of the polymers, producing novel structured materials with enhanced properties.[28−31] For

Received: February 28, 2014
Published: June 13, 2014

   dx.doi.org/10.1021/ja502075f | *J. Am. Chem. Soc.* 2014, 136, 9982−9989

instance, when the NPs are segregated at the interface between the two different polymer domains, they can function as surfactants, thereby improving the interfacial properties and inducing dramatic morphological transition.[32−38] Thus, the NPs in the BCPs can be effective surfactants for tailoring both the shape and the inner structure of the BCP particles with high stability, driven by their quasi-irreversible adsorption to the interface.[35,39−41] Particularly, the role of the NP surfactants should be emphasized in determining the shape and inner morphology of the BCP particles as the interfacial interactions are greatly magnified by the high surface area of the emulsion particles relative to their volume. However, examples of precise positioning of the NP arrays in the BCP particles are very limited.[11]

Herein, we report a novel and powerful strategy of using size-controlled NP surfactants to control the internal morphology as well as the overall shape of the BCP particles. The nonconventional structure of the convex lens-shaped particles (*CL* particles) with highly ordered and oriented nanoporous channels were generated through the combination of confined geometry by emulsion templation and interfacial modulation using Au NPs as surfactants. The key to the successful generation of these novel structures is the use of size-controlled Au NPs, in which the relative size ratio of Au NPs (d) over the Au NP-hosting domain (L), i.e. d/L, was critical for their precise positioning to determine their ability to function as surfactants in emulsions.[13,26,42,43] The size-dependent assembly of the Au NPs was localized preferentially at the interface between one block domain (P4VP) of the BCPs at the particle surface and the surrounding water, which enabled the modulation of the interfacial properties at selective locations on the BCP particles. Unlike the previous pure BCP particles with anisotropic shapes,[9,44−50] these *CL* particles had the unprecedented, convex lens shaped structures. Also, they had regularly ordered channels that can provide a functional space in which a variety of materials can be loaded (e.g., metals and dyes), thereby significantly increasing the versatility of the *CL* particles for various practical applications. For example, *CL* particles with highly ordered Au rods were prepared by filling the channels with Au, exhibiting the unique optical property as a microlens, which was well matched with the finite-difference time domain (FDTD) simulation.

RESULTS AND DISCUSSION

Scheme 1 illustrates the creation of *CL* particles from the mixture of polystyrene-*b*-poly(4-vinylpyridine) (PS-*b*-P4VP) BCPs and oleylamine-capped Au NPs using the 'emulsion-encapsulation and evaporation process'. In order to generate strong favorable interaction between the NPs and the BCP chains, we introduced 3-*n*-pentadecylphenol (PDP) as the small-molecule linkers with the P4VP block of the PS-*b*-P4VP chains, the pyridine group of which is known to interact with the phenol group of the PDP via hydrogen bonds, forming a PS-*b*-P4VP(PDP) comb-like supramolecule.[24,51] First, PS-*b*-P4VP BCPs were dissolved in chloroform to produce a 1 wt % polymer solution. Then, the PDP molecules in chloroform were added to the PS-*b*-P4VP solution with 0.5 feed ratio of 4VP to PDP units (PS-*b*-P4VP(PDP)$_{0.5}$). After adding Au NPs with various volume fractions (ϕ_{Au}) of the NPs,[52] the PS-*b*-P4VP(PDP)$_{0.5}$ solutions were emulsified in deionized water containing 0.5 wt % of cetyltrimethylammonium bromide (CTAB) using a homogenizer in order to produce BCP particles with Au NPs.

Scheme 1. Schematic Illustration of the Fabrication of Convex Lens-Like BCP Particles with Highly-Ordered Porous Channels Driven by Size-Controlled Au NPs; When Size-Controlled Au NPs (d = 1.9 to 8.1 nm) Were Added to the PS$_{50k}$-*b*-P4VP$_{13k}$(PDP)$_{0.5}$ Solution (L = 22.3 nm), only the Large Au NPs Moved to the Outer Surface of the BCP Particle during Emulsification, Inducing the Morphological Transition

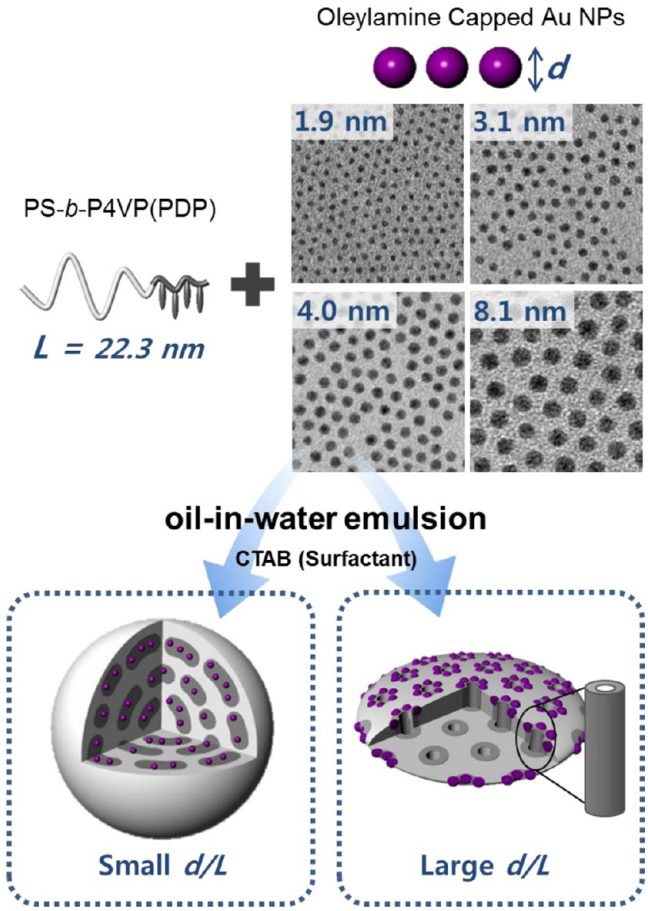

Images a and b of Figure 1 show scanning electron microscopy (SEM) images and transmission electron microscopy (TEM) images of PS$_{27k}$-*b*-P4VP$_{7k}$(PDP)$_{0.5}$ particles without Au NPs. The spherical BCP particles with cylindrical internal morphology were formed with preferential wetting of the PS layer to the particle surface because of the strong, nonfavorable interaction of the P4VP(PDP)$_{0.5}$ domains with the CTAB surfactants at the particle surface. Surprisingly, the addition of a small amount of Au NPs (diameter (d) = 4 nm, feed volume fraction of Au NPs (ϕ_{Au}) = 0.02) led to an interesting change in the overall shape of the BCP particles from spherical to a convex lens shape with hexagonally packed dimples on the both the top and bottom surfaces (SEM image of Figure 1c). The internal morphology of the *CL* particles was characterized by TEM images (Figure 1d). For all of the particles, the dark P4VP(PDP)$_{0.5}$ annulus domains were arranged hexagonally, which indicated that the standing-up cylindrical channels were developed inside the particle.

To gain deeper insight into the morphology of the *CL* particles and the spatial distribution of Au NPs, the *CL* particles were characterized by tilted TEM images. As shown in Figure 2a, the mean diameter of the pores, the P4VP(PDP)$_{0.5}$ annulus,

dx.doi.org/10.1021/ja502075f | J. Am. Chem. Soc. 2014, 136, 9982−9989

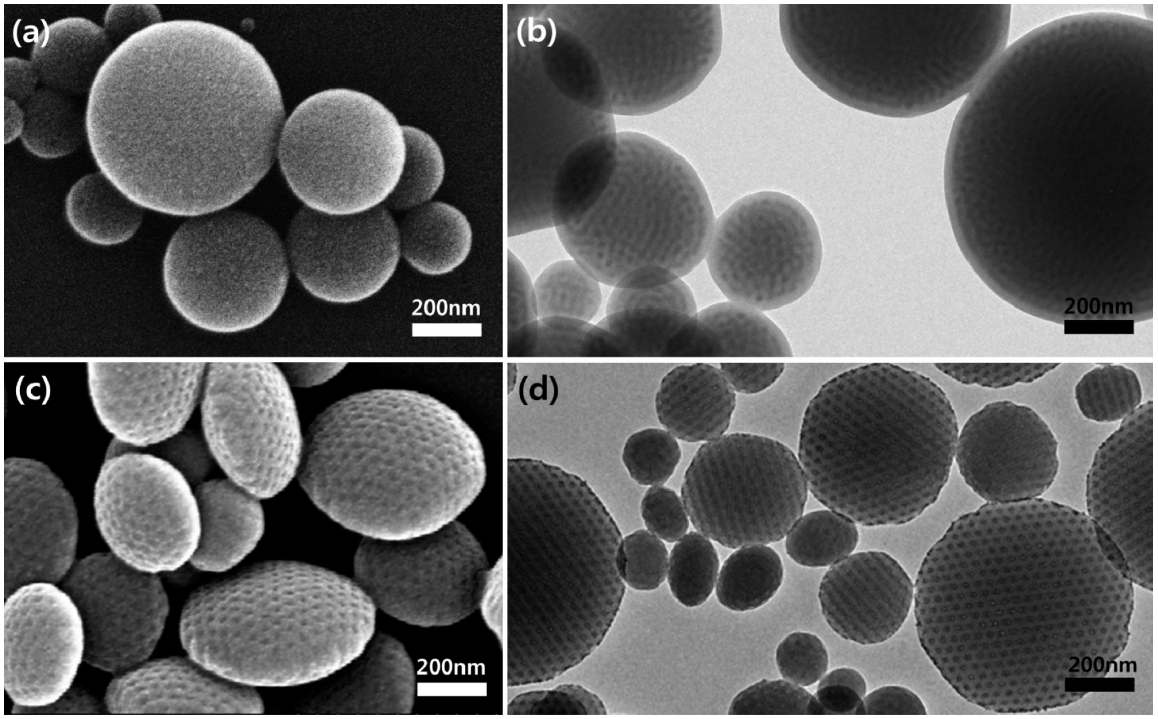

Figure 1. (a) SEM and (b) TEM images of PS_{27k}-*b*-$P4VP_{7k}(PDP)_{0.5}$ BCP particles without Au NPs. The BCP particles were spherical in shape and had cylindrical internal morphology. (c) SEM and (d) TEM images of PS_{27k}-*b*-$P4VP_{7k}(PDP)_{0.5}$ particles including 4 nm size Au NPs at $\phi_{Au} = 0.02$. Convex lens-shaped particles (*CL* particles) with regular porous structures were fabricated. The PS domains are the gray parts, and the P4VP domains appeared as darker rings after staining with iodine vapor.

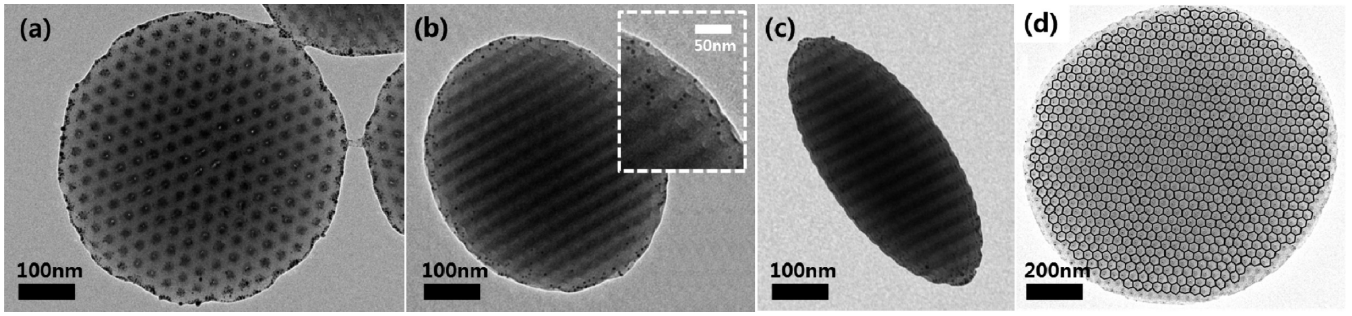

Figure 2. TEM images of PS_{27k}-*b*-$P4VP_{7k}(PDP)_{0.5}$ BCP particles with the Au NPs tilted at angles of (a) 0°, (b) 25°, and (c) 60°. Regularly arranged dimple structures were observed at the surface of the particles, and the Au NPs were located around the dark gray ring (P4VP domain) of the surface of the BCP particles. (d) Voronoi diagram constructed from the locations of the P4VP domain center in the *CL* particle.

and the center-to-center distance between pores were measured at 6.1 ± 0.4 nm, 21.6 ± 1.7 nm, and 42.3 ± 3.4 nm, respectively. It is notable that the cylinders with pores were well-oriented and highly ordered within the BCP particles. This feature is evidently shown in the Voronoi diagram in Figure 2d, in which the center of every domain has six nearest neighbors, and this high degree of lateral order was found to extend over the entire area of all of the particles. In addition, when the *CL* particles were tilted at an angle of 25°, it was clearly observed that the segregation of Au NPs were only at the $P4VP(PDP)_{0.5}$ domain on their surfaces. The regularly ordered, dimple structures were observed at the surface of the particles, and the Au NPs were preferentially located at the interface between the P4VP domain of the particle and the surrounding medium of the particle (water). When the *CL* particles were tilted at 60° (Figure 2c), the vertical cylinders were overlapped; thus, the axially stacked morphology of PS and $P4VP(PDP)_{0.5}$ was observed. (The entire tomography TEM movie of the *CL* particles being tilted from −30° to +60° is in the Supporting Information (SI).) Thus, the porous cylinders were highly oriented, ordered, and persisted throughout the entire thickness of the BCP particles. Additional evidence of the segregation of the Au NPs at the border of the *CL* particles was provided by the cross-sectional TEM images (SI Figure S2a and b).

Scheme 2 illustrates the hypothetical mechanism by which the *CL* particles are formed by the Au NP surfactants. During the emulsification step, large Au NPs moved to the BCP emulsion/water interface. Therefore, the BCP particles are stabilized by dual surfactants of Au NPs and CTAB molecules (Scheme 2a). It is well-known that the Au NPs have strong favorable interactions with the P4VP(PDP) domain of the BCPs, while the CTAB molecules interact preferably with the PS chains of the BCPs.[11,15,24] Thus, the Au NPs and CTAB surfactants, which are mobile at the emulsion/water interface, rearrange themselves to phase separate by interacting two different domains of the PS-*b*-P4VP(PDP), respectively, at the

dx.doi.org/10.1021/ja502075f | *J. Am. Chem. Soc.* 2014, 136, 9982−9989

Scheme 2. Schematic Illustration of the Formation Mechanism of BCP *CL* Particles from an Emulsion Droplet of Chloroform

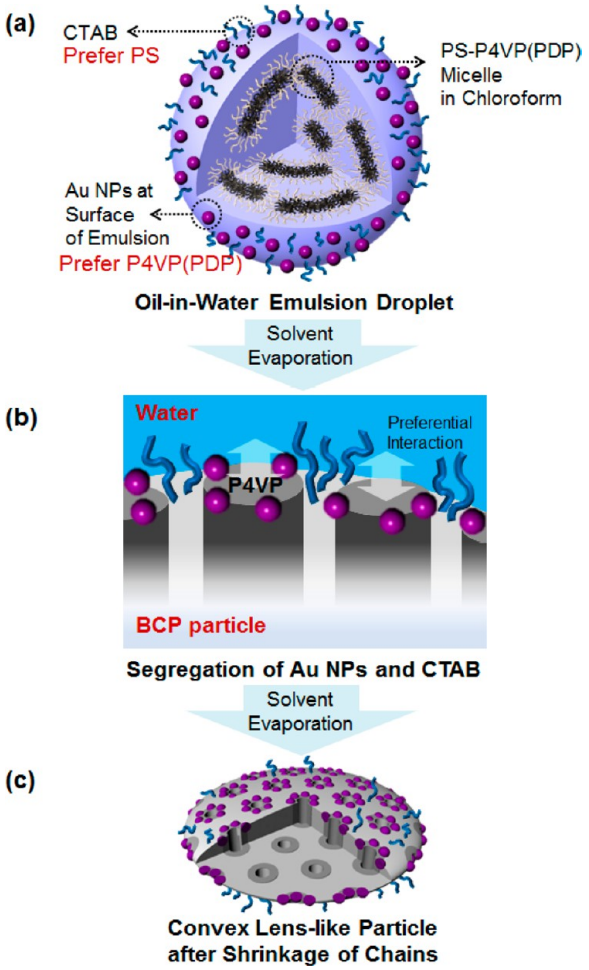

emulsion surface.[9] This could generate a balanced interfacial interaction between the two different PS/P4VP domains of the BCP particles and surrounding water,[11] leading to the nucleation of PS-*b*-P4VP(PDP) from the particle surface (Scheme 2b). When the solvent (chloroform) evaporates, the particles are still dispersed in water, so the hydrophilic P4VP chains strongly interact with the surrounding water. Thus, because of both strong unfavorable interactions between the PS and P4VP blocks, and preferential interaction between P4VP and water, the defects in the hexagonal packing of the cylindrical microdomains are rapidly removed. Consequently, long-range lateral order of the hexagonal BCP morphology is achieved in the particle.[49,53−55] During further evaporation of the chloroform, the BCP particles shrink in the vertical direction due to the enthalpic penalty associated with the migration of the BCP chains through the immiscible domains. Also, for the system of hexagonal phase with orientation perpendicular to the boundaries, lower free energy is expected when the particles have a convex lens shape rather than a spherical one.[44,45] When all of the water, which once swelled the P4VP(PDP)$_{0.5}$ cylinders, has been removed, small PDP molecules are extracted with water by disassembly from P4VP domain, followed by surface reconstruction of P4VP domains. This process produces cylindrical pores inside the P4VP domains of the particles (Scheme 2c).[10] The interfacial activity of Au NP surfactants at the emulsion/water is critical for the generation of the *CL* particles.

Precise positioning of Au NPs within the BCP particles (i.e., segregation of Au NPs to the border of the particles) can be achieved by tuning the relative size-ratio of Au NPs to the Au NP-hosting domain (d/L).[13,26,42,43] To quantitatively investigate the effect of d/L value on the morphology of the BCP particles, we increased the P4VP domain size by using higher-molecular weight PS$_{50k}$-*b*-P4VP$_{13k}$ polymers, and we varied the size of the Au NPs from 3 nm (d/L = 0.14) to 8 nm (d/L = 0.36). Parts a−f in Figure 3 are TEM and SEM images of PS$_{50k}$-*b*-P4VP$_{13k}$ BCP particles mixed with Au NPs that had the same ϕ_{Au} value of 0.02 but different sizes of 3 and 8 nm, respectively. The 3 nm Au NPs were incorporated and well dispersed within the P4VP(PDP)$_{0.5}$ domain, and the spherical shape of the particles was well maintained, because in this case, CTAB molecule is a sole surfactant to produce the BCP particles. In contrast, for the 8 nm Au NPs with the same ϕ_{Au} value of 0.02, *CL* particles were fabricated with the decoration of the Au NPs at the particle surface. When P4VP(PDP)$_{0.5}$ domain was large enough (low d/L value), the Au NPs were incorporated into the P4VP(PDP)$_{0.5}$ domain due to the strong favorable interaction between the aliphatic chain of PDP and the oleylamine ligands on the surface of the Au NPs.[10,24] In contrast, for the addition of the larger 8 nm Au NPs (high d/L value), the entropic penalty associated with the stretching of BCP chains to host large-sized Au NPs became the dominant factor in determining the location of the Au NPs, thus driving them to be excluded from the P4VP(PDP)$_{0.5}$ domain. Also, the oleylamine ligands at the less-curved surface of the larger Au NPs are expected to be more densely packed, which could reduce their favorable interaction with the PDP molecules and lead to steric exclusion of the Au NPs from the P4VP(PDP) domain. These phenomena can be well predicted on the basis of the results previously observed in the bulk system[56] and the thin film.[26,57] For instance, Xu et al. reported size-dependent assemblies of NP mixtures including one-dimensional chain and three-dimensional array in BCP thin films by tuning the d/L ratio.[26] In our case, the Au NPs were segregated at the outer surface of the BCP particles, thereby modulating the interfacial interactions by attracting P4VP to the emulsion/water interface.

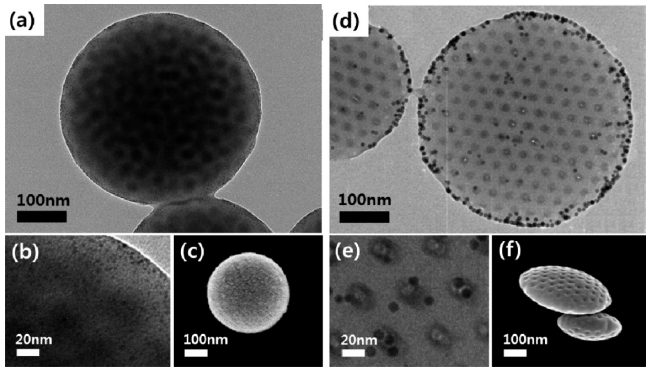

Figure 3. TEM and SEM images of PS$_{50k}$-*b*-P4VP$_{13k}$(PDP)$_{0.5}$ particles including Au NPs with different sizes of 3 nm (a, b, and c) and 8 nm (d, e, and f). ϕ_{Au} value was fixed at 0.02. For the 3 nm Au NPs, the Au NPs were incorporated in the P4VP domain, which maintained its overall spherical shape. In contrast, for the 8 nm Au NPs with the same ϕ_{Au}, the *CL* particles were fabricated.

dx.doi.org/10.1021/ja502075f | *J. Am. Chem. Soc.* 2014, 136, 9982−9989

When the surface properties and the size of the Au NPs were precisely controlled, the NP volume fraction, ϕ_{Au} had significant influence on the distribution of the NP location within the BCP domain; thus, ϕ_{Au} can drive the morphological transition of the BCP particles.[56,58] With that in mind, we fixed the size of the Au NPs at 4 nm but varied ϕ_{Au} from 0 to 0.172. At low ϕ_{Au} values ($\leq$0.02), the BCP particles remained spherical, and most of the Au NPs were located within the P4VP(PDP) domain inside the BCP particles (a and b of Figure 4). In contrast, at the high ϕ_{Au} value of 0.111, all of the

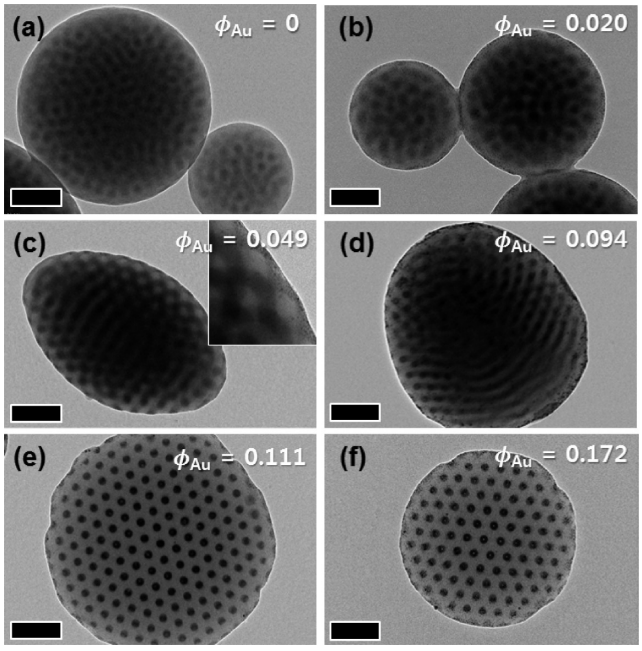

Figure 4. TEM images of PS_{50k}-*b*-$P4VP_{13k}(PDP)_{0.5}$ BCP particles including Au NPs (d = 4 nm) with various ϕ_{Au} values of (a) 0, (b) 0.020, (c) 0.049, (d) 0.094, (e) 0.111, and (f) 0.172. The size of the Au NPs was fixed at 4 nm. The scale bar is 100 nm. By increasing the volume fraction of the Au NPs, the morphology was transformed from spherical to a mixed morphology. Finally, *CL* particles with vertically highly ordered cylinders were obtained at ϕ_{Au} values greater than 0.111.

BCP particles had convex lens-like shape with porous cylinder channels (Figure 4e and f). Again, the porous structures showed a remarkably high degree of lateral order without any defects. It is worthwhile to note that in this case (d/L = 0.19), the critical ϕ_{Au} value ($(\phi_{Au})_c$) required to produce the morphological transition to *CL* particles was found to be a much higher ϕ_{Au} value. As shown in Figure 4, a $(\phi_{Au})_c$ value of 0.111 was required, whereas a $(\phi_{Au})_c$ value of only 0.02 was required in the previous system in which a larger d/L of 0.36 was used (Figure 3d). At the regime with intermediate values of ϕ_{Au}, we observed an interesting morphological behavior of the BCP particles. When the ϕ_{Au} value increased greater than 0.02, the shape of BCP particles started to deform to an ellipsoidal shape (Figure 4c). Moreover, the BCP particles included a mixture of radially and axially ordered cylinders (Figure 4d), which was very different from the disordered internal structures of the BCP particles at very low ϕ_{Au} values. For the BCP particles that had the mixed morphologies, some Au NPs were observed at the surfaces of the particles, but the quantities of the Au NP surfactants segregated at the surface of the BCP particles were not sufficient to produce *CL* particles.

The morphological behavior of PS_{50k}-*b*-$P4VP_{13k}(PDP)_{0.5}$ particles containing Au NPs is summarized in Figure 5 in

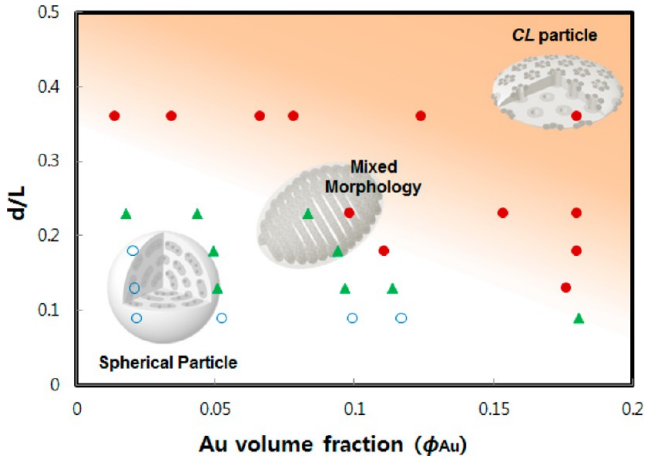

Figure 5. Summary of the morphological transition of PS_{50k}-*b*-$P4VP_{13k}(PDP)_{0.5}$ BCP particles plotted by d/L value vs ϕ_{Au}, where d is the diameter of Au NPs, and L is size of the P4VP domain: (red ●) *CL* particle; (green ▲) mixed morphology; and (blue ○) spherical particle.

terms of d/L and ϕ_{Au} values. In the phase diagram, the red-filled circles indicate the formation of *CL* particles. For example, when the d/L value was fixed at 0.19, the transition window to form *CL* particles was $0.094 \leq (\phi_{Au})_c \leq 0.111$. For comparison, at a larger d/L value (~0.36), a tiny amount of Au NPs ($(\phi_{Au})_c < 0.02$) are sufficient to induce the morphological transition to the *CL* particles, because all of the Au NPs were segregated to the outer interface between the BCP particles and water, where they acted as a surfactant. In contrast, at the small d/L value of ~0.1, no morphological transition of the BCP particles was observed even at very large ϕ_{Au} values exceeding 0.18 (SI Figure S3). It is evident from these results that the d/L value determines both the internal morphology and the shape of the BCP particles.

These *CL* particles can possess interesting optical properties by themselves, such as strong light scattering due to their convex lens-like shape. Thus, they can be applicable as a microlens in which light can be concentrated toward the focal point. When we performed finite-difference time-domain (FDTD) simulation to calculate the near-field signals around the *CL* particle as a collimated beam was injected to the particle, it was found that the intensity of the electric field was focused at one point above the particle. (SI Figure S5a) Moreover, the highly ordered porous channels in the *CL* particles can provide interesting opportunities for adding versatility to their practical applications. For example, the channels potentially could be utilized as a directed-release drug delivery system, which would function by the diffusion of the drug thorough the nanometer-sized channel. Also, they can be used as the nanoreactors for generating a variety of inorganic nano-objects (i.e., uniformly shaped, rod-type NPs), because the nitrogen−metal ion complexes in the P4VP chains could serve as nucleation sites for the growth of NPs.[59−63] To this end, various metal precursors, including Au, Ag, and Pt, were loaded within the *CL* particles, producing the hybrid *CL* particles containing highly ordered metal-containing cylinders in order to significantly increase the versatility of the hybrid *CL* particles and explore the full potential of their defect-free hybrid

dx.doi.org/10.1021/ja502075f | *J. Am. Chem. Soc.* 2014, 136, 9982−9989

channel structures. Figure 6 shows the hybrid *CL* particle with highly ordered Au NP-containing cylinders. Au precursors were

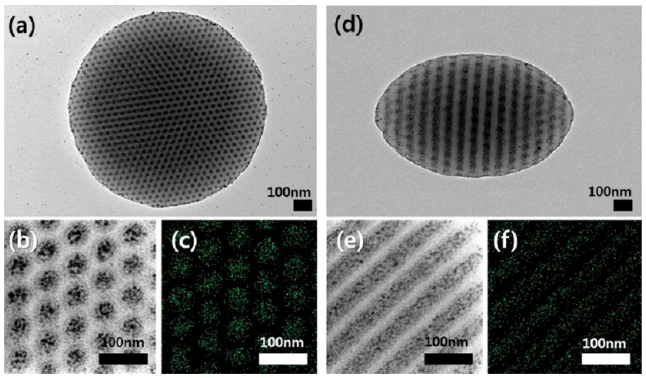

Figure 6. TEM images of PS_{27k}-*b*-$P4VP_{7k}(PDP)_{0.5}$ *CL* particles after loading Au in the P4VP channels, tilted at angles of 0° (a and b), and 45° (d and e). EDX mapping of Au (c and f).

incorporated by the *in situ* method, and the P4VP channels were selectively loaded with Au, as shown in Figure 6a. Energy-dispersive X-ray spectroscopy (EDX) measurements confirmed that the Au atoms were present only within the P4VP domains. The TEM image (Figure 6b) and corresponding electron mapping image (Figure 6c) of Au NP-containing *CL* particles revealed the selective incorporation of Au into the P4VP chains. By tilting the particles at an angle of 45°, the incorporation of Au precursors inside the channels of all of the P4VP cylinders was evidently observed, as shown in d–f of Figure 6. In a similar manner, Figure S4 in the SI shows the successful incorporation of other precursors, such as Ag and Pt, into the P4VP channels of the BCP particles.

Metallic nanostructures, such as Au and Ag, can manipulate light beyond the optical diffraction limit due to the collective electron oscillations known as surface plasmons.[64−66] The combination of the plasmonic property of metals and a well-ordered BCP geometry can exhibit a unique optical property for organic/inorganic hybrid material. In particular, when the metal has well-defined geometry with high ordering as *CL* particles, the electromagnetic fields can be concentrated into a deep subwavelength-scale area, and these highly localized fields can provide extreme enhancement in the light intensity.[66,67] We experimentally investigated the plasmonic property of the particles with a near-field scanning optical microscope (NSOM), and made a comparison with FDTD simulations theoretically by calculating the distributions of near-field signals at the surface of *CL* particles. An AFM topography image of single *CL* particle and the corresponding near-field signal distribution are shown in parts a and b of Figure 7, respectively. It should be noted that stronger near-field signals were clearly observed both at the edge of the particle and at the center of the surface plane. This unique near-field signal could be understood by FDTD simulation. In the simulation, Au was modeled with the Drude-critical points model, and a monochromatic plane wave (λ = 532 nm) was incident from the bottom SiO_2 substrate where the incident light was linearly polarized along the *x*-axis. Parts c and d of Figure 7 show the calculated electric field distribution of the scattering signal from the individual *CL* particle along the *z*-axis and 40 nm away from the surface of *CL* particle, respectively. Comparing the NSOM signal in Figure 7b with the simulation result by cross sectioning along the dashed line in Figure 7c, both showed

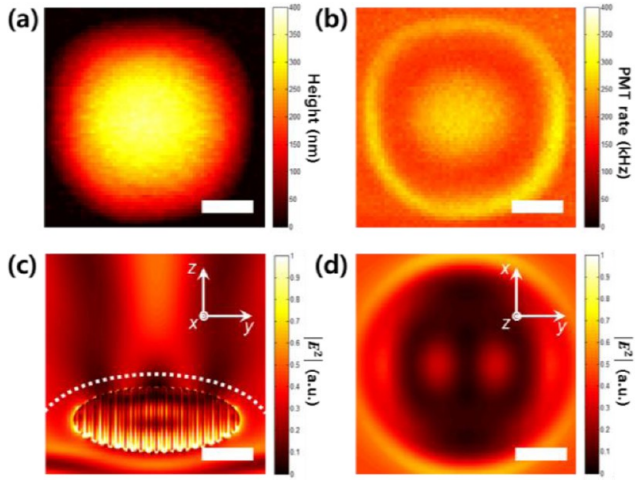

Figure 7. Optical properties of the hybrid PS_{27k}-*b*-$P4VP_{7k}(PDP)_{0.5}$ *CL* particle containing highly ordered Au NP-containing cylinders. (a) AFM image of individual CL particle; (b) near-field distribution at the surface of the particle observed by NSOM, which corresponds to the AFM image in (a); and calculated electric field intensity distribution by FDTD simulation along (c) *z*-axis, and (d) 40 nm away from the surface of the particle (dashed line in c). The scale bars are 300 nm.

the greater intensities at the edge and the center. Interestingly, in contrast to the hybrid *CL* particle containing cylindrical Au, the convex lens-shaped pristine polymer particle did not show any unique near-field distribution at the surface of the particle (SI Figure S5). Therefore, the bright center and ring indicate the enhanced intensity of the signal, which arises from the array of the vertically ordered Au-containing cylinders.

CONCLUSION

A simple, yet powerful, strategy of using size-controlled NPs was developed in order to control both the external shape and the internal nanoscale morphology of colloidal particles. Convex lens-shaped BCP particles with defect-free, porous channels were created by tuning the interfacial properties at selective locations on the particles using size-dependent assemblies of the Au NP surfactants. The power of using size-controlled Au NPs as surfactants is apparent as the internal morphology and the shape of the BCP particles could be characterized by tilted and cross-sectional TEM images and a tomographic movie. The size-induced segregation of the Au NP surfactants at the mobile boundary of the BCP particle/water interface produced vertically highly ordered, porous P4VP cylinders inside the *CL* particles. Moreover, *CL* particles including metal-containing rods could be fabricated by loading various metal precursors into the highly ordered channels in the P4VP cylinders. Well-ordered Au rods within the *CL* particle made it possible to concentrate light toward the focused point above the particle, as well as possess a unique distribution of electromagnetic field at the particle surface, allowing superb applications of such particles in the nano-optical sensing and imaging fields.

ASSOCIATED CONTENT

Supporting Information

Full experimental procedures. Additional TEM images and FDTD simulation results, and the tomography movie of BCP particles with Au NPs. This material is available free of charge via the Internet at http://pubs.acs.org.

dx.doi.org/10.1021/ja502075f | *J. Am. Chem. Soc.* 2014, 136, 9982−9989

AUTHOR INFORMATION

Corresponding Authors

bumjoonkim@kaist.ac.kr (B.J.K.)
segyujang@kepri.re.kr (S.G.J.)

Notes

The authors declare no competing financial interest.

ACKNOWLEDGMENTS

This research was supported by a Korea Research Foundation Grant (2013R1A2A1A03069803), and by the Global Frontier R&D Program on Center for Multiscale Energy System (2012M3A6A7055540), funded by the Korean Government. This work was also supported by Samsung Research Funding Center of Samsung Electronics under Project Number SRFC-MA1301-07. We thank Prof. Ryan Hayward for helpful discussions.

REFERENCES

(1) Arsenault, A. C.; Rider, D. A.; Tétreault, N.; Chen, J. I. L.; Coombs, N.; Ozin, G. A.; Manners, I. *J. Am. Chem. Soc.* **2005**, *127*, 9954.

(2) Li, L.; Matsunaga, K.; Zhu, J.; Higuchi, T.; Yabu, H.; Shimomura, M.; Jinnai, H.; Hayward, R. C.; Russell, T. P. *Macromolecules* **2010**, *43*, 7807.

(3) Shin, K.; Xiang, H.; Moon, S. I.; Kim, T.; McCarthy, T. J.; Russell, T. P. *Science* **2004**, *306*, 76.

(4) Wu, Y.; Cheng, G.; Katsov, K.; Sides, S. W.; Wang, J.; Tang, J.; Fredrickson, G. H.; Moskovits, M.; Stucky, G. D. *Nat. Mater.* **2004**, *3*, 816.

(5) Bockstaller, M. R.; Kolb, R.; Thomas, E. L. *Adv. Mater.* **2001**, *13*, 1783.

(6) Setaro, A.; Lettieri, S.; Maddalena, P.; De Stefano, L. *Appl. Phys. Lett.* **2007**, *91*, 051921.

(7) Robb, M. J.; Connal, L. A.; Lee, B. F.; Lynd, N. A.; Hawker, C. J. *Polym. Chem.* **2012**, *3*, 1618.

(8) Lu, Z. H.; Liu, G. J.; Phillips, H.; Hill, J. M.; Chang, J.; Kydd, R. A. *Nano Lett.* **2001**, *1*, 683.

(9) Jeon, S. J.; Yi, G. R.; Yang, S. M. *Adv. Mater.* **2008**, *20*, 4103.

(10) Deng, R.; Liu, S.; Li, J.; Liao, Y.; Tao, J.; Zhu, J. *Adv. Mater.* **2012**, *24*, 1889.

(11) Jang, S. G.; Audus, D. J.; Klinger, D.; Krogstad, D. V.; Kim, B. J.; Cameron, A.; Kim, S. W.; Delaney, K. T.; Hur, S. M.; Killops, K. L.; Fredrickson, G. H.; Kramer, E. J.; Hawker, C. J. *J. Am. Chem. Soc.* **2013**, *135*, 6649.

(12) Klinger, D.; Wang, C. X.; Connal, L. A.; Audus, D. J.; Jang, S. G.; Kraemer, S.; Killops, K. L.; Fredrickson, G. H.; Kramer, E. J.; Hawker, C. J. *Angew. Chem., Int. Ed.* **2014**, DOI: 10.1002/anie.201400183.

(13) Thompson, R. B.; Ginzburg, V. V.; Matsen, M. W.; Balazs, A. C. *Science* **2001**, *292*, 2469.

(14) Spontak, R. J.; Shankar, R.; Bowman, M. K.; Krishnan, A. S.; Hamersky, M. W.; Samseth, J.; Bockstaller, M. R.; Rasmussen, K. O. *Nano Lett.* **2006**, *6*, 2115.

(15) Kim, B. J.; Bang, J.; Hawker, C. J.; Kramer, E. J. *Macromolecules* **2006**, *39*, 4108.

(16) Li, W.; Liu, S.; Deng, R.; Zhu, J. *Angew. Chem., Int. Ed.* **2011**, *50*, 5865.

(17) Li, W.; Zhang, P.; Dai, M.; He, J.; Babu, T.; Xu, Y. L.; Deng, R.; Liang, R.; Lu, M. H.; Nie, Z.; Zhu, J. *Macromolecules* **2013**, *46*, 2241.

(18) Jang, S. G.; Khan, A.; Hawker, C. J.; Kramer, E. J. *Macromolecules* **2012**, *45*, 1553.

(19) Bockstaller, M. R.; Mickiewicz, R. A.; Thomas, E. L. *Adv. Mater.* **2005**, *17*, 1331.

(20) Haryono, A.; Binder, W. H. *Small* **2006**, *2*, 600.

(21) Walther, A.; Matussek, K.; Muller, A. H. E. *ACS Nano* **2008**, *2*, 1167.

(22) Arora, H.; Du, P.; Tan, K. W.; Hyun, J. K.; Grazul, J.; Xin, H. L.; Muller, D. A.; Thompson, M. O.; Wiesner, U. *Science* **2010**, *330*, 214.

(23) Shenhar, R.; Norsten, T. B.; Rotello, V. M. *Adv. Mater.* **2005**, *17*, 657.

(24) Zhao, Y.; Thorkelsson, K.; Mastroianni, A. J.; Schilling, T.; Luther, J. M.; Rancatore, B. J.; Matsunaga, K.; Jinnai, H.; Wu, Y.; Poulsen, D.; Frechet, J. M. J.; Alivisatos, A. P.; Xu, T. *Nat. Mater.* **2009**, *8*, 979.

(25) Chiu, J. J.; Kim, B. J.; Kramer, E. J.; Pine, D. J. *J. Am. Chem. Soc.* **2005**, *127*, 5036.

(26) Kao, J.; Bai, P.; Lucas, J. M.; Alivisatos, A. P.; Xu, T. *J. Am. Chem. Soc.* **2013**, *135*, 1680.

(27) Kao, J.; Thorkelsson, K.; Bai, P.; Rancatore, B. J.; Xu, T. *Chem. Soc. Rev.* **2013**, *42*, 2654.

(28) Yeh, S. W.; Wei, K. H.; Sun, Y. S.; Jeng, U. S.; Liang, K. S. *Macromolecules* **2003**, *36*, 7903.

(29) Li, L.; Miesch, C.; Sudeep, P. K.; Balazs, A. C.; Emrick, T.; Russell, T. P.; Hayward, R. C. *Nano Lett.* **2011**, *11*, 1997.

(30) Balazs, A. C.; Emrick, T.; Russell, T. P. *Science* **2006**, *314*, 1107.

(31) Ikem, V. O.; Menner, A.; Bismarck, A. *Angew. Chem., Int. Ed.* **2008**, *47*, 8277.

(32) Chung, H.; Ohno, K.; Fukuda, T.; Composto, R. J. *Nano Lett.* **2005**, *5*, 1878.

(33) Chung, H.; Kim, J.; Ohno, K.; Composto, R. J. *ACS Macro Lett.* **2012**, *1*, 252.

(34) Kim, B. J.; Fredrickson, G. H.; Hawker, C. J.; Kramer, E. J. *Langmuir* **2007**, *23*, 7804.

(35) Kang, D. J.; Kwon, T.; Kim, M. P.; Cho, C. H.; Jung, H.; Bang, J.; Kim, B. J. *ACS Nano* **2011**, *5*, 9017.

(36) Stratford, K.; Adhikari, R.; Pagonabarraga, I.; Desplat, J. C.; Cates, M. E. *Science* **2005**, *309*, 2198.

(37) Cates, M. E.; Clegg, P. S. *Soft Matter* **2008**, *4*, 2132.

(38) Niu, Z. W.; He, J. B.; Russell, T. P.; Wang, Q. A. *Angew. Chem., Int. Ed.* **2010**, *49*, 10052.

(39) Lin, Y.; Daga, V. K.; Anderson, E. R.; Gido, S. P.; Watkins, J. J. *J. Am. Chem. Soc.* **2011**, *133*, 6513.

(40) Bockstaller, M. R.; Thomas, E. L. *Phys. Rev. Lett.* **2004**, *93*, 166106.

(41) Binks, B. P. *Curr. Opin. Colloid Interface Sci.* **2002**, *7*, 21.

(42) Spontak, R. J.; Shankar, R.; Bowman, M. K.; Krishnan, A. S.; Hamersky, M. W.; Samseth, J.; Bockstaller, M. R.; Rasmussen, K. Ø. *Nano Lett.* **2006**, *6*, 2115.

(43) Bockstaller, M. R.; Lapetnikov, Y.; Margel, S.; Thomas, E. L. *J. Am. Chem. Soc.* **2003**, *125*, 5276.

(44) Yang, S. M.; Kim, S. H.; Lim, J. M.; Yi, G. R. *J. Mater. Chem.* **2008**, *18*, 2177.

(45) Champion, J. A.; Katare, Y. K.; Mitragotri, S. *Proc. Natl. Acad. Sci. U.S.A.* **2007**, *104*, 11901.

(46) Kim, M. P.; Kang, D. J.; Jung, D. W.; Kannan, A. G.; Kim, K. H.; Ku, K. H.; Jang, S. G.; Chae, W. S.; Yi, G. R.; Kim, B. J. *ACS Nano* **2012**, *6*, 2750.

(47) Ku, K. H.; Kim, M. P.; Paek, K.; Shin, J. M.; Chung, S.; Jang, S. G.; Chae, W.-S.; Yi, G.-R.; Kim, B. J. *Small* **2013**, *9*, 2667.

(48) Jeon, S. J.; Yi, G. R.; Koo, C. M.; Yang, S. M. *Macromolecules* **2007**, *40*, 8430.

(49) Park, S. C.; Kim, B. J.; Hawker, C. J.; Kramer, E. J.; Bang, J.; Ha, J. S. *Macromolecules* **2007**, *40*, 8119.

(50) Mei, S. L.; Wang, L.; Feng, X. D.; Jin, Z. X. *Langmuir* **2013**, *29*, 4640.

(51) Ruokolainen, J.; Saariaho, M.; Ikkala, O.; ten Brinke, G.; Thomas, E. L.; Torkkeli, M.; Serimaa, R. *Macromolecules* **1999**, *32*, 1152.

(52) Peng, S.; Lee, Y. M.; Wang, C.; Yin, H. F.; Dai, S.; Sun, S. H. *Nano Res.* **2008**, *1*, 229.

(53) Kim, S. H.; Misner, M. J.; Xu, T.; Kimura, M.; Russell, T. P. *Adv. Mater.* **2004**, *16*, 226.

(54) Bang, J.; Kim, S. H.; Drockenmuller, E.; Misner, M. J.; Russell, T. P.; Hawker, C. J. *J. Am. Chem. Soc.* **2006**, *128*, 7622.

(55) Park, S.; Wang, J. Y.; Kim, B.; Xu, J.; Russell, T. P. *ACS Nano* **2008**, *2*, 766.

(56) Kim, B. J.; Fredrickson, G. H.; Bang, J.; Hawker, C. J.; Kramer, E. J. *Macromolecules* **2009**, *42*, 6193.
(57) Kao, J.; Bai, P.; Chuang, V. P.; Jiang, Z.; Ercius, P.; Xu, T. *Nano Lett.* **2012**, *12*, 2610.
(58) Chiu, J. J.; Kim, B. J.; Yi, G. R.; Bang, J.; Kramer, E. J.; Pine, D. J. *Macromolecules* **2007**, *40*, 3361.
(59) Hayward, R. C.; Chmelka, B. F.; Kramer, E. J. *Adv. Mater.* **2005**, *17*, 2591.
(60) Chai, J.; Wang, D.; Fan, X. N.; Buriak, J. M. *Nat. Nanotechnol.* **2007**, *2*, 500.
(61) Koh, H. D.; Park, S.; Russell, T. P. *ACS Nano* **2010**, *4*, 1124.
(62) Spatz, J. P.; Herzog, T.; Mossmer, S.; Ziemann, P.; Möller, M. *Adv. Mater.* **1999**, *11*, 149.
(63) Sohn, B. H.; Seo, B. H. *Chem. Mater.* **2001**, *13*, 1752.
(64) Barnes, W. L.; Dereux, A.; Ebbesen, T. W. *Nature* **2003**, *424*, 824.
(65) Stöckle, R. M.; Suh, Y. D.; Deckert, V.; Zenobi, R. *Chem. Phys. Lett.* **2000**, *318*, 131.
(66) Eustis, S.; El-Sayed, M. A. *Chem. Soc. Rev.* **2006**, *35*, 209.
(67) Chen, H. J.; Shao, L.; Li, Q.; Wang, J. F. *Chem. Soc. Rev.* **2013**, *42*, 2679.